Geophys. J. Int. (1997) **131**, 281–292

The onset of Pleistocene glaciation in the Barents Sea: implications for glacial isostatic adjustment

Georg Kaufmann
Research School of Earth Sciences, Australian National University, Canberra ACT 0200, *Australia. E-mail: georg@rses.anu.edu.au*

Accepted 1997 June 16. Received 1997 June 3; in original form 1996 September 1

SUMMARY

In this paper the effect of a delayed onset of glaciation in the Barents Sea on glacial isostatic adjustment is investigated. The model calculations solve the sea-level equation governing the total mass redistributions associated with the last glaciation cycle on a spherically symmetric, linear, Maxwell viscoelastic earth for two different scenarios for the growth phase of the Barents Sea ice sheet. In the first ice model a linear growing history is used for the Barents Sea ice sheet, which closely relates its development to the build-up of other major Late Pleistocene ice sheets. In the second ice model the accumulation of the Barents Sea ice sheet is restricted to the last 6 ka prior to the last glacial maximum.

The calculations predict relative sea levels, present-day radial velocities, and gravity anomalies for the area formerly covered by the Weichselian ice sheet. The results show that observed relative sea levels in the Barents Sea are appropriate for distinguishing between the different glaciation histories. In particular, present-day observables such as the free-air gravity anomaly over the Barents Sea, and the present-day radial velocities are sensitive to changes in the glaciation history on this scale.

A palaeobathymetry derived from relative sea-level predictions before the last glacial maximum based on the second ice model essentially agrees with a palaeobathymetry derived by Lambeck (1995). The additional emerged areas provide centres for the build-up of an ice sheet and thus support the theory of Hald, Danielsen & Lorentzen (1990) and Mangerud *et al.* (1992) that the Barents Sea was an essentially marine environment shortly before the last glacial maximum.

Key words: Barents Sea ice sheet, glacial rebound, gravity anomalies, isostasy, sea level, viscoelasticity.

1 INTRODUCTION

The deformation of the Earth due to surface loads can be related to a variety of forces, which cover a broad range on the timescale. On the short timescale daily ocean tides with periods of hours perturb the sea level. Atmospheric pressure changes due to local weather phenomena force perturbations on the same timescale. A common feature of these short-term forces is that the sea level is not in equilibrium, because the forces are not in phase with the sea-level change. On the long timescale the sea level is in equilibrium; here perturbations of the sea level are mainly forced by internal and external mass redistributions in and on the Earth. On the far end of the timescale plate tectonics induces movements of the continents and therefore changes the shape and the bathymetry of the oceans over millions of years.

A prominent force perturbing the sea level on a timescale of 10^3–10^5 years is the growth and decay of large ice sheets during glacial epochs. Changes in the space–time history of these ice sheets and the related fluctuations of ocean mass due to the meltwater taken from or added to the ice sheets result in global isostatic adjustment of the Earth. This is recorded in ancient shorelines, either below or above the present mean sea level, in ongoing uplift of formerly glaciated areas and subsidence of large areas in the equatorial oceans, and in perturbations of the Earth's geoidal surface, resulting in glaciation-induced gravity anomalies.

Simulations of the deformation of the Earth due to changes in the global distribution of ice sheets are mostly interested in the space–time history of the *deglaciation* process, besides the interior structure of the Earth. In these studies it is common to replace the growth phase of the ice sheets by an

infinite glaciation phase, resulting in a state of isostatic equilibrium prior to deglaciation (Peltier & Andrews 1976; Peltier & Tushingham 1989; Tushingham & Peltier 1991). Notable exceptions using a finite growth phase for models of ice sheets are Wu & Peltier (1983), Nakada & Lambeck (1987) and Mitrovica, Davis & Shapiro (1994).

In Mitrovica & Davis (1995), for the first time the importance of a *finite glaciation phase* was studied systematically. The authors discuss three different glaciation histories for the Late Pleistocene ice-sheet distribution prior to the last glacial maximum (hereafter 'LGM'). They concluded that a finite glaciation cycle can significantly influence the prediction of relative sea levels and gravity anomalies, when compared to calculations adopting an infinite glaciation phase. Additionally, the authors obtained notable differences from the above-mentioned predictions for different *global* glaciation histories, especially when the main growth phase of the ice sheets was restricted to a period close to the LGM.

It is still debatable whether *all* Late Pleistocene ice sheets could have accumulated in the final phase before the LGM as suggested in Chappell & Shackleton (1986) and assumed in Mitrovica & Davis (1995). However, there is one notable exception, the Barents Sea ice sheet. While the other large ice sheets such as the Laurentide and the Fennoscandian ice sheets are *continent*-based ice sheets, the Barents Sea and Kara Sea ice sheets are *marine*-based ice sheets. As previously discussed in Elverhøi *et al.* (1993), the growth of a marine-based ice sheet is more difficult to explain than the growth of a continental ice sheet. Unlike the latter, which will start growing by expanding mountain glaciers onto the continent, a marine-based ice sheet needs areas above sea level to start growing. A mechanism outlined in Denton & Hughes (1981), which is redrawn in Kaufmann & Wolf (1996), explains the onset with the formation of gradually thickening, floating sea ice, which finally forms an ice shelf. Based on this shelf an ice dome can be built up. As the initially floating sea ice can thermally isolate the water below, and oceanic currents prevent water from freezing (Elverhøi *et al.* 1993), the above-mentioned process must be supported by additional effects.

Recent investigations of Hald *et al.* (1990), based on shallow sea cores of the southwestern Barents Sea, and Mangerud *et al.* (1992) suggest a marine environment in the Barents Sea as late as 23 ka BP. During that time parts of the shallow Barents Sea shelf now below sea level could have been above sea level due to the global sea-level fall of about 125 m (Fairbanks 1989) and therefore provide additional areas for the onset of ice growth. This in fact has been shown by Lambeck (1995), who has derived a palaeobathymetry of the Barents Sea from calculations of sea-level change due to deformation associated with the growth and decay of Pleistocene ice sheets. He concluded that in the *absence* of an ice sheet over the Barents Sea during the last glacial cycle, a substantial part of the Barents Sea shelf would have been either very shallow or even above sea level.

In the present paper we investigate the effect of a *delayed onset* of the glaciation in the Barents Sea on the isostatic adjustment in northern Europe. Therefore, we derive two global ice models describing the space–time history of the Late Pleistocene ice-sheet distribution, which both adopt a finite glaciation phase, but differ in the time of the onset of the Barents Sea ice sheet. We predict relative sea levels, present-day radial velocities and free air gravity anomalies and additionally compare the predicted water depths for these models with the ones previously published in Lambeck (1995).

The main purposes of this paper are thus to answer the following questions. (1) Can a Barents Sea ice sheet, which starts accumulating during the last phase of the glaciation just prior to the LGM, significantly influence either regional or global isostatic adjustment? (2) Which observables are most sensitive for inferring the characteristics of the onset of the glaciation cycle?

These two objectives will be achieved using a numerical model to predict 3-D deformations on a spherically symmetric, self-gravitating earth subject to global mass redistributions. Therefore, in Section 2 we introduce ice and earth models and a set of relative sea-level observations used in this approach. In Section 3 we briefly outline the theoretical model on which the calculations are based. The results of the calculations are discussed in Section 4 and are summarized in Section 5.

2 INPUT DATA

In this section we introduce the ice models used and we briefly describe the physical properties of the earth models. Both the ice and the earth models are regarded as prescribed in this approach, which is sufficient due to the objectives raised in the Introduction. The validity of the ice model used for modelling postglacial isostatic adjustment has been shown previously in the literature (Tushingham & Peltier 1991, 1992).

2.1 Ice models

Modelling 3-D deformations on a spherically symmetric earth due to global mass redistributions related to the Late Pleistocene glacial cycle requires a global description of the space–time history of the major ice sheets during that period. We have based our approach on the ice model Ice-3G (Tushingham & Peltier 1991), which has been derived from predictions of relative sea-level changes at sites located within the formerly glaciated areas under the assumption of an infinite glaciation phase. The LGM for this ice model is at 18 ka BP (sidereal time); the deglaciation was modelled by a set of Heaviside functions with 1 ka intervals. Deglaciation was finished at around 4 ka BP. The Weichselian part of the ice model at the LGM is redrawn in Fig. 1, showing a continental ice dome over Fennoscandia and a marine-based ice dome over the central Barents Sea.

We have modified the glaciation and deglaciation history of the Ice-3G model to match the following constraints.

(1) A finite glaciation phase has been adopted similar to the one described in Mitrovica & Davis (1995) to simulate the onset of the last glaciation cycle as well as the glaciation of the Barents Sea.

(2) The corresponding times of the Ice-3G deglaciation phase have been readjusted to match the results arising from the recalibration of the ^{14}C timescale (e.g. Bard *et al.* 1990). In their paper Bard *et al.* (1990) have shown that the ^{14}C ages are systematically younger than the more accurate U/Th ages. Although the Ice-3G times are sidereal, this shift in the timescale was not accounted for. We adopt a polynomial function for the recalibration given by Han & Wahr (1995). Applying the correction yields a LGM at around 22 ka BP.

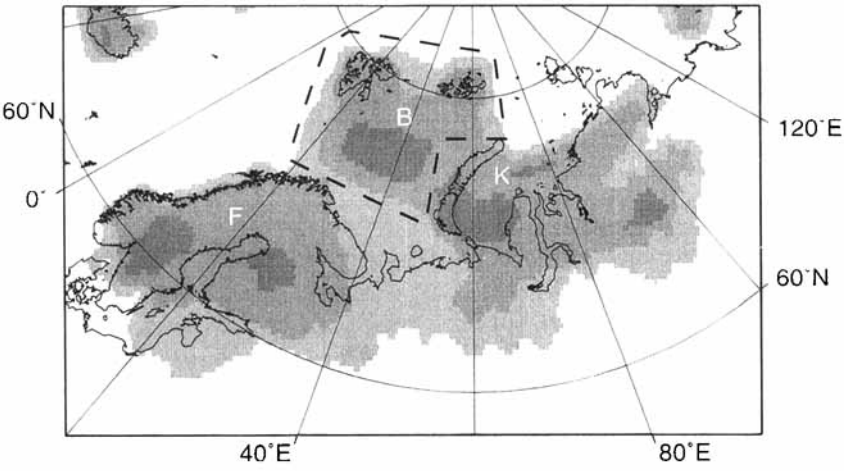

Figure 1. Ice model Ice-3G at the LGM over Fennoscandia (F) and the Barents (B) and Kara seas (K). Contour interval for load thickness is 1000 m starting at load margin. The area enclosed by the dashed line is delayed during the glaciation phase for the ice model ONSET2.

(3) We have used a linear change in the ice-load history between the given times, using a modified Heaviside function (e.g. Johnston 1993).

Particular attention has been paid to the finite glaciation phase. As in Mitrovica & Davis (1995), we have used the Ice-3G load heights of the deglaciation intervals to model the finite glaciation phase. Therefore the corresponding times have been converted backwards in time from the LGM with time increments set every 6 ka BP, starting with the Ice-3G time 17 ka BP, which matches the glaciation time 24 ka BP. Note that these times are still subject to the recalibration, which in this case will give a time at around 28 ka BP. Stepping further back in time, we finally arrive at the onset of the glaciation cycle at around 105 ka BP (recalibrated time). We refer to that ice model as ice model ONSET1.

ONSET1 results in a glaciation phase in which the spatial distribution is similar to that of the deglaciation phase. An alternative approach with a glaciation phase based on geomorphological and glaciological constraints would be more accurate, but this would require a more detailed knowledge of the onset of the Late Pleistocene glaciation in space and time, which is not available at present.

To investigate the effects of a delayed onset of the glaciation of the Barents Sea as mentioned in Elverhøi *et al.* (1993), we have excluded the area enclosed by the dashed line in Fig. 1 from the glaciation phase of ice model ONSET1. In ice model ONSET2, this area, matching the marine-based Barents Sea ice sheet, has started growing at around 24 ka BP (28 ka BP recalibrated time), reaching its largest dimensions at the LGM together with the other major ice sheets. Thus, ice model ONSET2 ensures that the Barents Sea was essentially a marine environment as late as 28 ka BP (recalibrated time) as suggested by Mangerud *et al.* (1992) and Elverhøi *et al.* (1993).

2.2 Earth models

We have adopted five-layer, compressible Maxwell viscoelastic earth models for all calculations in this study. The elastic structure is derived from the seismically based model PREM (Dziewonski & Anderson 1981) and is redrawn in Fig. 2. The viscosity is given by a step function as a function of the earth's radius. All earth models consist of an elastic lithosphere, a layered, viscoelastic mantle, and an inviscid core. The free parameters are the viscosities of the upper and lower mantle,

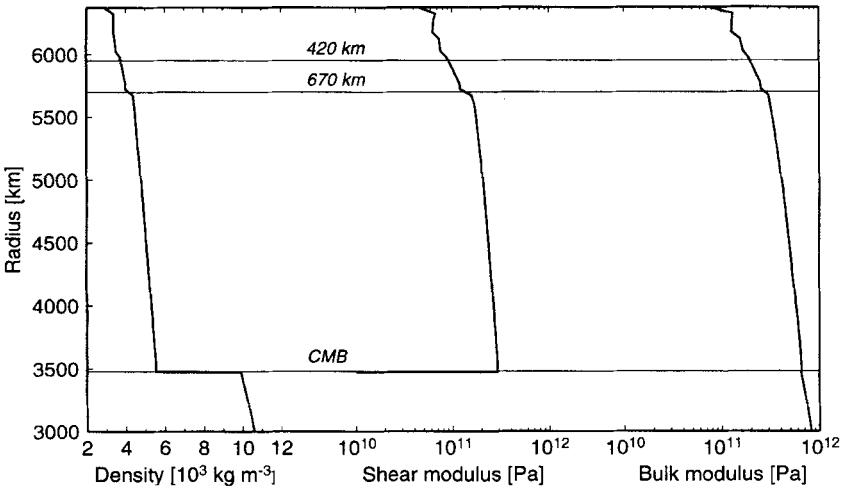

Figure 2. Elastic properties of compressible Maxwell-viscoelastic earth models.

Table 1. Key for viscosity stratification in earth models.

	74	84	91	94	95	99
η_{UM}	4×10^{20}	7×10^{20}	10^{21}	10^{21}	10^{21}	10^{21}
η_{LM}	7×10^{21}	7×10^{21}	10^{21}	7×10^{21}	10^{22}	10^{23}

termed η_{UM} and η_{LM}, respectively, and the thickness of the elastic lithosphere, termed h. The abbreviation earth model x/y refers to a model with $h=x$ km and y as defined in Table 1.

2.3 Relative sea level

Ancient shorelines, which may be found either above or below the present mean sea level, are indicators of global mass redistributions on the Earth. If the redistributions are related to the melting of the large Late Pleistocene ice sheets with their transfer of mass from the (mostly) continent-based ice sheets to the ocean and internal mass redistributions in the Earth's mantle due to isostatic adjustment, dated shoreline elevations (hereafter RSL sites) can be used as a constraint to infer both the interior structure of the Earth and the space–time distribution of Late Pleistocene ice sheets.

When both the earth and the ice models are regarded as prescribed as in this approach, the effects of the onset of glaciation, using different ice models, on postglacial isostatic adjustment can be studied. For this purpose we have chosen 15 RSL sites distributed over Northern Europe, which are sampled to cover all areas of interest related to the former Weichselian ice sheet (Fig. 3). The first five RSL sites are located within the area of the Fennoscandian ice dome, with Varanger Fjord (1) and Ingøy (2) at the northern margin, Ångermanland (4) at the centre and Frosta (3) and Oslo (5) at the western and southern margins of the former ice sheet. The RSL sites Agardhbukta (6), Barentsøya (7), Billefjorden (8), Daudmannsøyra (9), Hopen (10), Kong Karls Land (11), Murchisonfjorden (12), Wilhelmsøya (13) and Ytterdalen (14) sample the area of the Svalbard Archipelago fairly evenly. The RSL site Rhine Delta (15) is located outside the formerly glaciated area. The dated shoreline elevations of sites 1–5 and 15 are taken from a global database compiled by Tushingham & Peltier (1991) and sites 6–14 are collected from a database used in Kaufmann & Wolf (1996). The uncertainties of the ages and elevations of sites 1–5 and 15 are described in Tushingham & Peltier (1992); for sites 6–14 they are taken from Kaufmann (1995).

3 THEORETICAL MODEL

In this section we briefly outline the mathematical approach used to infer 3-D deformations on a spherically symmetric earth due to global mass redistributions. Starting with the deformation of a spherically symmetric *elastic* earth induced by impulsive surface loads (e.g. Farell 1972), we find the associated Green's functions for a number of field quantities, for example the radial displacement and the potential perturbation. Applying the correspondence principle (e.g. Biot 1962) to the elastic equations, we arrive at Green's functions describing the deformation of a *linear viscoelastic* earth due to impulsive surface loads, for example the Green's functions of the radial displacement, the potential perturbation at the deformed surface due to load and internal mass redistributions,

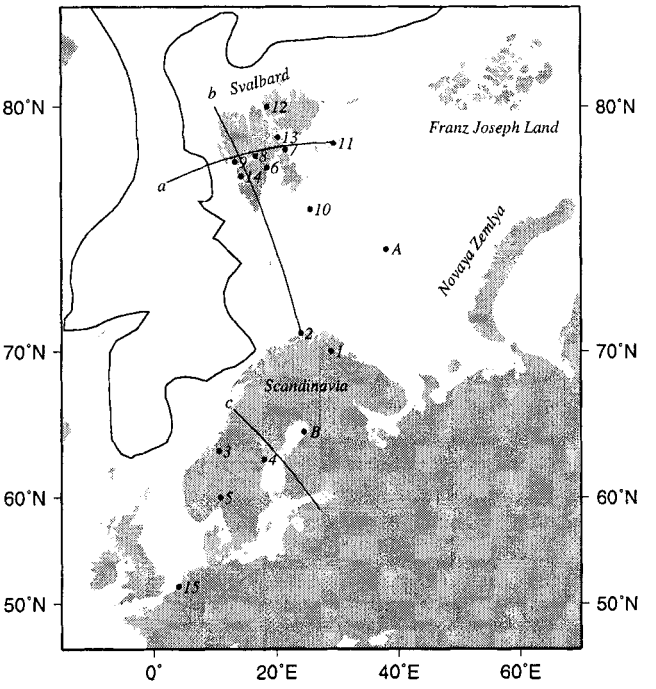

Figure 3. Location map of Scandinavia and the Barents Sea showing RSL sites Varanger Fjord (1), Ingøy (2), Frosta (3), Ångermanland (4), Oslo (5), Agardhbukta (6), Barentsøya (7), Billefjorden (8), Daudmannsøyra (9), Hopen (10), Kong Karls Land (11), Murchisonfjorden (12), Wilhelmsøya (13), Ytterdalen (14), Rhine Delta (15) and uplift profiles Fram Strait–Kong Karls Land (a), Yermak Plateau–Ingøy (b) and NW Norway–Estonia (c). The locations for the free air gravity anomaly are indicated by *A* (Barents Sea) and *B* (Gulf of Bothnia). The thick solid line indicates the 1000 m isobath of the continental margin.

and the free air gravity anomaly (e.g. Farrell and Clark 1976; Mitrovica & Peltier 1989; Han & Wahr 1995):

$$G_U(\gamma,t)=\frac{a}{m_e}\sum_{l=0}^{\infty}h_l(t)P_l(\cos\gamma), \tag{1}$$

$$G_\Phi(\gamma,t)=\frac{ag}{m_e}\sum_{l=0}^{\infty}[\delta(t)+k_l(t)-h_l(t)]P_l(\cos\gamma), \tag{2}$$

$$G_{FA}(\gamma,t)=-\frac{g}{m_e}\sum_{l=0}^{\infty}[(l+2)\delta(t)-(l-1)k_l(t)]P_l(\cos\gamma), \tag{3}$$

where a is the Earth's radius, m_e is the Earth's mass, g is the gravitational acceleration at the Earth's surface, δ is the Kronecker delta, P_l is the Legendre polynomial of degree l and γ is the angular distance between an observation point (θ,φ) and an impulsive load point (θ',φ') with θ and φ the colatitude and the eastern longitude and

$$\gamma=\cos\theta\cos\theta'+\sin\theta\sin\theta'\cos(\varphi-\varphi'). \tag{4}$$

The functions $h_l(t)$ and $k_l(t)$ are *dimensionless Love numbers* of the radial displacement and the potential perturbation due to an applied impulsive surface load (e.g. Love 1911; Longman 1962; Peltier 1974).

We continue defining a *surface load*, L, which is a function of the geographical location (θ,φ) and time t,

$$L(\theta,\varphi,t)=\rho_i I(\theta,\varphi,t)+\rho_w W(\theta,\varphi,t). \tag{5}$$

Here ρ_i and ρ_w denote the densities of ice and water, I is the prescribed space–time history of the ice model, and W is the *equilibrium ocean load*.

Based on (1)–(4) we can calculate the *response*, R, of a spherically symmetric viscoelastic earth due to surface loading using

$$R_{\{U,\Phi,FA\}}(\theta,\varphi,t) = \int_{-\infty}^{t}\int_{0}^{2\pi}\int_{0}^{\pi} a^2 L(\theta',\varphi',t') G_{\{U,\Phi,FA\}}(\gamma, t-t') d\varphi' \sin\theta' d\theta' dt'. \quad (6)$$

When we regard both the earth model given by surface Love numbers h_l and k_l and the ice model I as prescribed, we can then calculate the time-dependent equilibrium ocean load W, which is the third input parameter needed to infer field quantities associated with the isostatic adjustment process using (6). We therefore define the equilibrium ocean load as the projection of the time-dependent sea level onto the oceans (e.g. Farrell & Clark 1976):

$$W(\theta,\varphi,t) = C(\theta,\varphi,t)\left[\frac{R_\Phi(\theta,\varphi,t)}{g} + \frac{\Delta\Phi(t)}{g}\right], \quad (7)$$

with the time-dependent *ocean function*, C, equalling 1 over the oceans and zero elsewhere (Munk & MacDonald 1960). We identify (7) as the *sea-level equation* with contributions arising (1) from the equipotential surface perturbation at the deformed surface derived from Brun's formula (e.g. Heiskanen & Moritz 1967) and (2) a time-dependent shift of the entire equipotential surface to ensure conservation of mass (Farrell & Clark 1976). These terms are represented by the first and second terms, respectively, in brackets on the right-hand side of (7).

To solve (7) numerically, several approaches have been introduced (e.g. Wu & Peltier 1983; Nakada & Lambeck 1987; Johnston 1993). We will adopt the pseudospectral approach outlined in Mitrovica & Peltier (1991); the reader should consult this paper for further information on this method.

4 INTERPRETATION

In this section we present results of our model calculations and discuss their implications for postglacial isostatic adjustment arising from the different ice models used. First, we focus our interest on the change in sea level, which is recorded in ancient shorelines. Then we proceed by discussing the influence of a delayed onset of the glaciation of the Barents Sea on present-day observables. In the last section we compare a palaeobathymetry derived from calculations using ice model ONSET2 with results published in Lambeck (1995).

4.1 Relative sea-level change

4.1.1 RSL site Barbados

The sea-level record from offshore drillings in the coral reefs at Barbados (Caribbean Sea) discussed in Fairbanks (1989) provides one of the best continuous records of sea-level change during the Late Pleistocene deglaciation phase, since the samples date back to the LGM. As the site is located far enough away from of all major Late Pleistocene ice sheets, the influence of mass redistributions related to the melting of these ice sheets is rather small, thus the sea-level record provides a rough global estimate of the eustatic sea-level rise since the LGM.

In Fig. 4 we have compared the dated observations obtained by U/Th mass spectrometry (Bard *et al.* 1990) with several calculated predictions of the relative sea-level change due to ice models ONSET1 and ONSET2. As a RSL site like Barbados is relatively insensitive to lithospheric thickness, we have chosen earth models with constant lithospheric thickness and varied the mantle-viscosity profile from a uniform viscosity of 10^{21} Pa s (120/91), a one order of magnitude increase (120/74) and a three orders of magnitude increase (120/99) across the 670 km discontinuity. We find that, independently of the ice model used, the relative sea level at the LGM can be explained by both models with uniform upper- and lower-mantle viscosities and a one order of magnitude increase. On the other hand, the large viscosity increase proposed by earth model 120/99 is somewhat less satisfactory. We note, however, that this result is strongly influenced by the total ice volume at the LGM, a quantity with reasonable uncertainties, especially for the Late Pleistocene ice sheets over the Barents Sea and Antarctica. The sea-level rise in late-glacial and Holocene times can be reasonably explained with all earth models, so no distinction between the different viscosity profiles is possible.

Observing the influence of the different ice models, we find that the delayed growth of the Barents Sea ice sheet (ONSET2) can be seen in the sea-level fall as early as 50 ka BP, independently of the earth model used. This result is closely related to the fact that the inversion of the Ice-3G deglaciation history for modelling the growth phase is used, with an early disappearance of the Barents Sea ice sheet at around 15 ka BP. The predicted sea-level fall between 50 ka BP and the LGM, then, is smaller for ONSET2, with an increased rate of change starting at about 30 ka BP close to the time that the onset of the growth of the Barents Sea ice sheet occurs in ONSET2.

We conclude that observations of relative sea-level change *prior* to the LGM can contribute to distinguishing between the two glaciation phases.

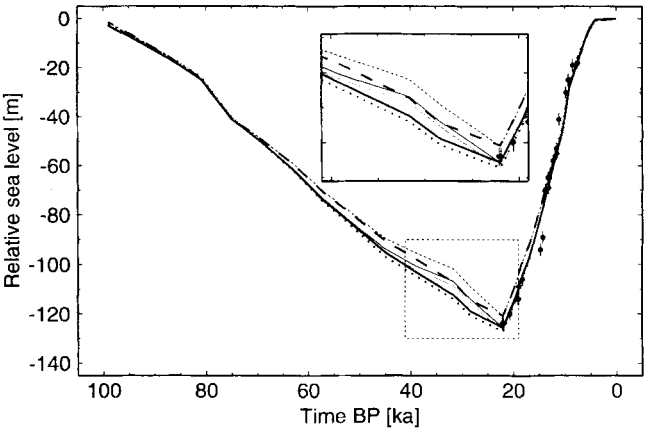

Figure 4. Observed and calculated relative sea level at Barbados (13°N, 60°W) for three different earth models and two ice models ONSET1 (thick lines) and ONSET2 (thin lines). Observations are represented by dots, uncertainties by bars and calculations by curves. Calculations apply to earth models 120/74 (solid lines), 120/91 (dotted lines) and 120/99 (dashed lines). The area enclosed by the dashed rectangle is shown in the enlargement.

4.1.2 *RSL sites in Europe*

We proceed by discussing predicted relative sea-level changes in northern Europe using the set of observed shoreline elevations introduced in Section 2.3. Additionally, we have calculated a misfit function, ϵ_s, for each RSL site, which is derived using a relation taken from Kaufmann & Wolf (1996). Here predicted and observed relative sea levels, $l_i^{(c)}$ and $l_i^{(o)}$, together with the uncertainty of the observed shoreline, Δl_i, are compared for shorelines at a single location, using

$$\epsilon_s = \sqrt{\frac{1}{I}\sum_{i=1}^{I}\left(\frac{l_i^{(c)} - l_i^{(o)}}{\Delta l_i}\right)^2}, \qquad (8)$$

where I is the number of shorelines at a specific location. We then calculated the mean misfit $\bar{\epsilon}$ for all sites ($s = 1, 15$) and the associated standard deviation, σ. The results are summarized in Table 2.

In Fig. 5 the relative sea-level predictions for earth models 120/74, 120/84, 120/94 and 70/84 and ice model ONSET1 are compared with observations. Starting with sites located in Scandinavia, we find that observations can be fitted best with earth models comprising a 120 km thick lithosphere and a moderate increase in mantle viscosity across the 670 km seismic discontinuity up to one order of magnitude. We note, however, that Late Pleistocene observations at Ingøy and Frosta are never correctly prediced. For the Rhine Delta (15), which is located in the southern forebulge area of the Fennoscandian ice sheet, all models predict the observations equally well except the oldest recorded shoreline. Thus, this site is not able to resolve rheological properties, but is useful in determining the total mass of the former ice sheet.

More care must be taken when explaining the relative sea-level change in the Svalbard Archipelago. Here RSL sites closer to the continental margin, such as Ågardhbukta (6), Billeforden (8), Daudmannsøyra (9), Murchisonfjorden (12) and Ytterdalen (14), as well as sites at an intermediate distance, such as Barentsøya (7) and Wilhelmsøya (13), clearly exclude a thinner lithosphere, while the two locations Hopen (10) and Kong Karls Land (11) can be fitted reasonably well with both thinner (70 km) and thicker (120 km) lithospheric thicknesses. In general, the best fit is achieved for earth model 120/74, which can also be seen in the mean misfit given in Table 2.

In Fig. 6 the predicted relative sea-level change for ice model ONSET2 is compared with the observations. We find that the delayed onset of the glaciation of the Barents Sea has nearly no influence on the relative sea level at sites in Scandinavia. Only RSL sites 1 and 2, located at the northern margin of the Fennoscandian ice sheet, exhibit a slight decrease in the predictions, not exceeding 8 per cent. RSL sites 3, 4 and 5 are almost insensitive to the choosen ice model. The same holds for RSL site 15 in the southern forebulge area. On the other hand, relative sea-level predictions in the Svalbard Archipelago are strongly influenced by the change in glaciation history. Predictions for ice model ONSET2 generally result in lower sea levels; now the predictions for earth model 120/74 are able to fit RSL sites 8, 9, 12, 13 and 14 better than the ones for ice model ONSET1. Only RSL sites 10 and 11 experience a less satisfactory fit to the observations. Thus we find that a delayed onset of glaciation in the Barents Sea is a possible scenario in terms of predictions of relative sea levels, but the ice height over the central Barents Sea has to be increased to fit observations in the southeastern part of the Svalbard Archipelago. The best mean misfit is again achieved for earth model 110/74; the misfit is now slightly smaller than for ice model ONSET1.

We conclude that a delayed onset of the glaciation in the Barents Sea significantly influences the predicted relative sea level in the area and therefore can be used as an additional constraint on the time history of this ice sheet in future investigations.

Table 2. Mean misfit $\bar{\epsilon}$ and associated standard deviation σ for four earth models (columns) and two ice models (rows) used in this approach.

	120/74	120/84	120/94	70/84
ONSET1	2.73 ± 0.42	3.15 ± 0.72	3.29 ± 0.75	8.01 ± 2.76
ONSET2	2.36 ± 0.42	2.42 ± 0.42	2.68 ± 0.40	5.78 ± 1.66

4.1.3 *RSL profiles in Europe*

In this section we discuss the significance of a delayed glaciation phase of the Barents Sea on predictions of relative sea-level change *prior* to the LGM. Therefore, in Fig. 7 predictions of relative sea-level change along three profiles, two in the western Barents Sea and one crossing the former centre of the Fennoscandian ice sheet (Fig. 3), are calculated for all earth and ice models at the time 28 ka BP, indicating the onset of glaciation in the Barents Sea in ice model ONSET2.

Along profile (a), predictions for all earth models and ice model ONSET1 yield raised shorelines east of the continental margin, with their maximum at the eastern edge of the profile (site 11). This relative sea-level rise is related to the early glaciation of the Barents Sea together with Scandinavia in ONSET1, resulting in a deformation which is nearly as large as at the LGM. West of the 1000 m isobath the shorelines are submerged.

The predictions for all earth models differ around 20 m west of the continental margin, and about the same amount east of the Svalbard Archipelago. In between, the differences are insignificant. Earth model 120/94 experiences the lowest sea-level rise around the eastern end of the profile, a result of the stiffer upper mantle.

Proceeding to the predictions of ice model ONSET2 along the profile, the situation changes totally. Now all earth models predict submerged shorelines along the entire profile, with 100–125 m along the western margin of the profile and therefore close to eustatic sea-level fall and even lower with approximately 130 m at the eastern margin of the profile (site 11). Here, additionally, the forebulge of the Fennoscandian ice dome contributes to the sea-level fall. The influence of the viscosity is now only significant along the western end of the profile, with differences of about 15 m between different earth models. We note that the relative sea-level fall observed for ONSET2 results in a rise of the bathymetry along the shallow banks in SE Svalbard as required for the onset of a marine-based ice sheet (see Section 1).

Profile (b) is chosen to sample the westernmost Barents Sea close to the continental margin, ranging from the Yermak Plateau NW of the Svalbard Archipelago to Ingøy at the northern coast of Norway. Observing the relative sea level for ice model ONSET1, we find raised shorelines for all earth models along the entire profile, with a maximum over the

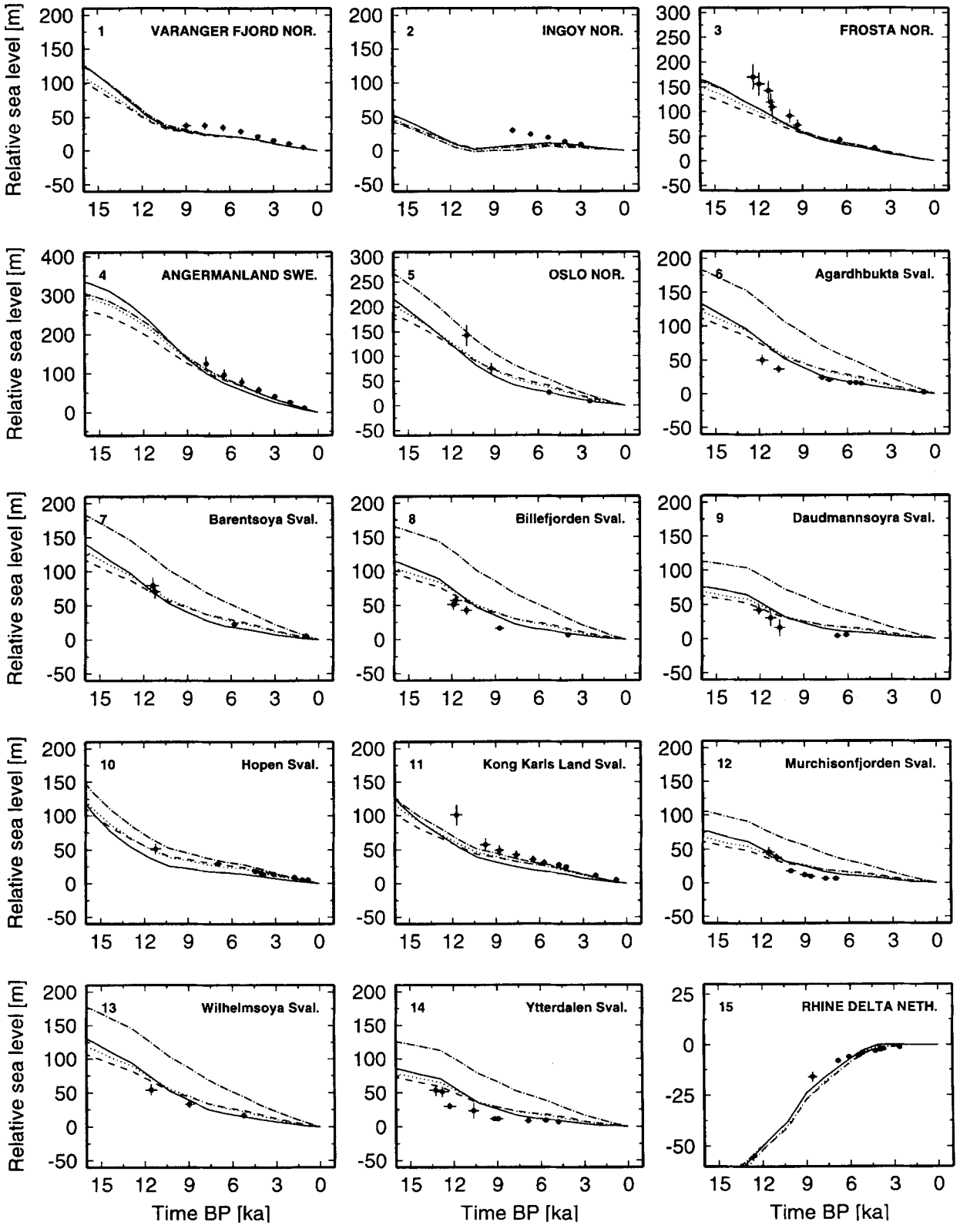

Figure 5. Observed and calculated relative sea level as a function of time before present (BP) for 15 locations. Observations are represented by dots, uncertainties by bars and calculations by curves. Calculations apply to ice model ONSET1 and earth models 120/74 (solid lines), 120/84 (dotted lines), 120/94 (dashed lines) and 70/84 (dash-dotted lines).

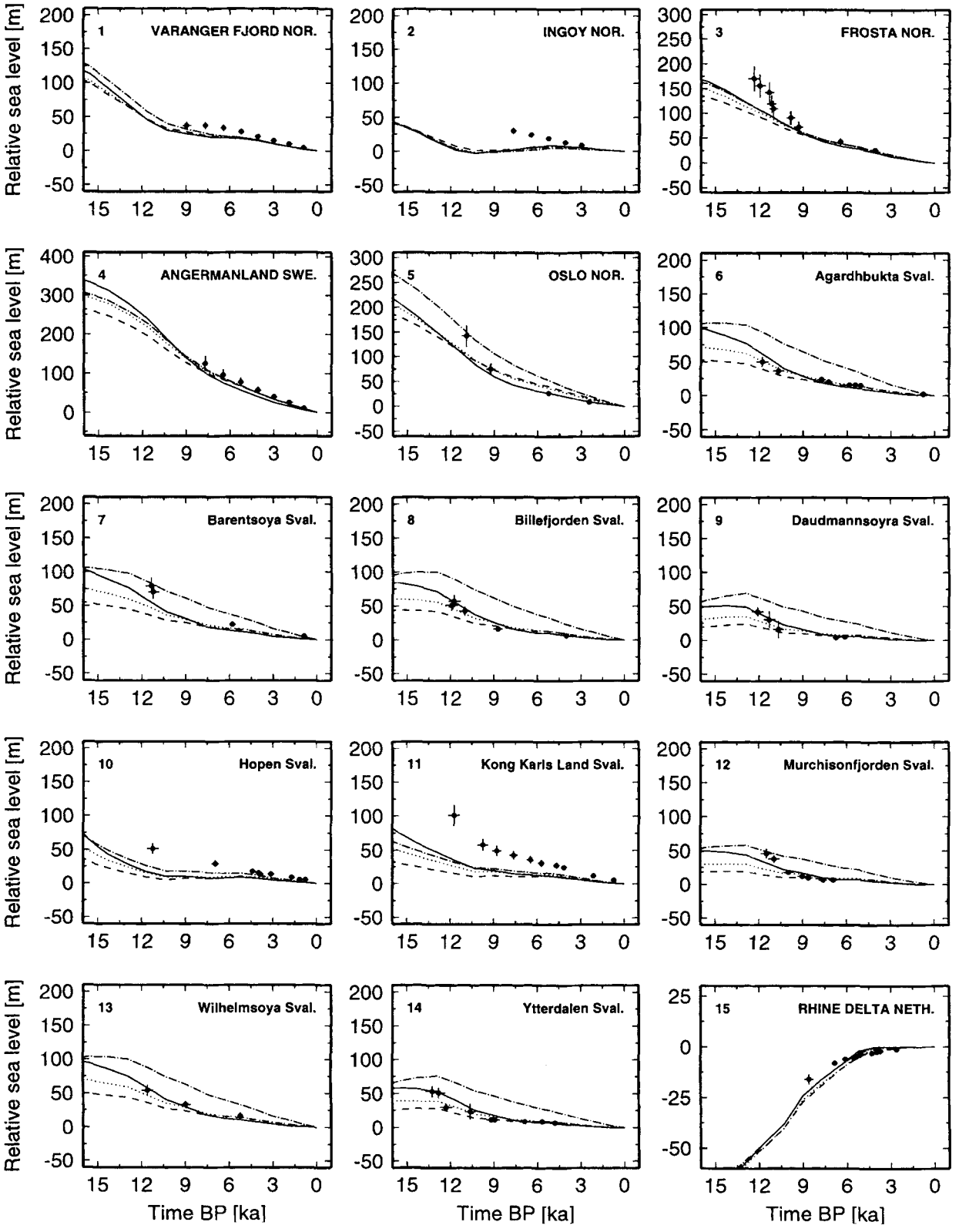

Figure 6. Same as Fig. 5, except that calculations apply to ice model ONSET2.

Isfjorden area (W Spitsbergen). Differences in relative sea-level predictions for all earth models are only minor, thus indicating a poor resolving power for the proposed differences in upper-mantle viscosity.

For ice model ONSET2 the situation changes along the entire profile. Now submerged shorelines can be observed along the Barents Sea for all earth models with the exception of the area just offshore the northern Norwegian coast. Here the

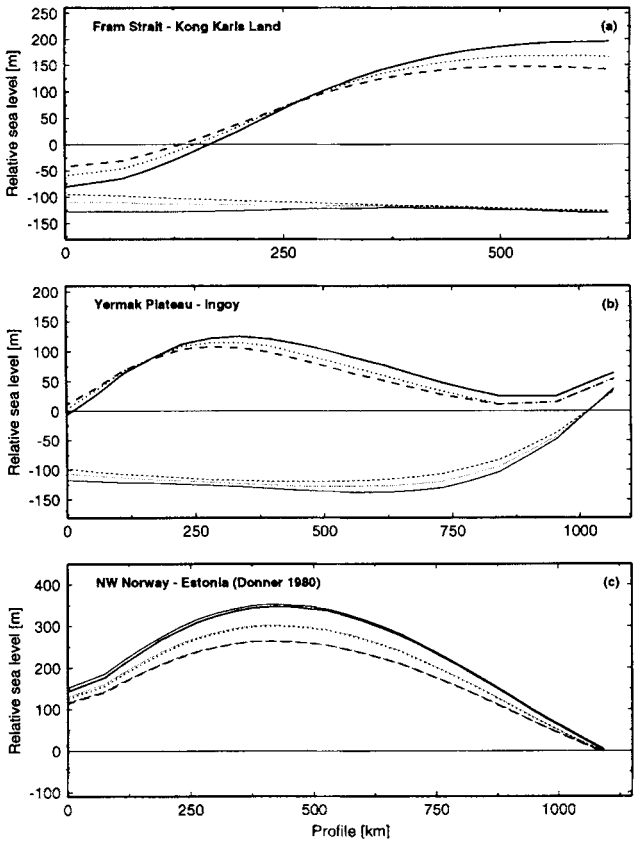

Figure 7. Calculated relative-sea-level change along three profiles at 28 ka BP for ice models ONSET1 and ONSET2 (thick and thin lines) and earth models 120/74 (solid lines), 120/84 (dotted lines) and 120/94 (dashed lines).

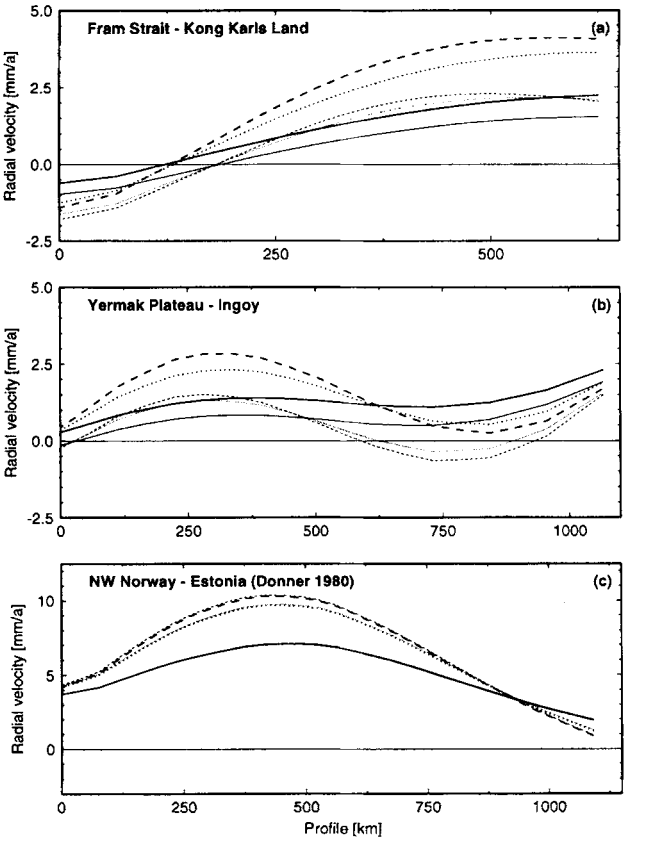

Figure 8. Calculated present radial velocities along three profiles for ice models ONSET1 and ONSET2 (thick and thin lines) and earth models 120/74 (solid lines), 120/84 (dotted lines) and 120/94 (dashed lines).

influence of the large Fennoscandian ice dome, causing raised shorelines, is obvious, resulting in raised shoreline elevations at similar or equal heights to those resulting from ice model ONSET1.

Continuing to profile (c), a profile similar to the one chosen by Donner (1980), stretching across the former Fennoscandian ice dome from W to E close to the centre, we observe well-raised shorelines for all earth models except at the far eastern end of the profile. Now the difference in shoreline elevation due to the different earth models is much more pronounced than in the two previous profiles, with a maximum difference of around 40 m between different earth models in the former centre of the Fennoscandian ice sheet. We note that the differences arising from the two different ice models are only minor.

We conclude that the effect of a delayed onset of glaciation in the Barents Sea is again a regional effect for shoreline elevations prior to the LGM, resulting in submerged instead of raised shorelines in the Barents Sea and no significant influence on shorelines in Scandinavia. Thus, observations older than the LGM are capable of distinguishing between the two proposed glaciation phases.

4.2 Present-day radial velocity

In this section we discuss the present-day radial velocities resulting from mass redistributions of the Late Pleistocene glaciation cycle. The calculations apply to the same three profiles as introduced in the last section (Fig. 8).

Along profile (a) the radial velocities are negative over the present oceanic areas and positive over the Svalbard Archipelago, thus showing the ongoing rebound of the islands and the collapse of the forebulge. The peak values over the eastern end of the profile do not exceed 2.5–4 mm a^{-1}, depending on the earth model, thus they are more than 50 per cent smaller than those predicted for other centres of formerly glaciated areas, for example 10 mm a^{-1} over the Gulf of Bothnia (Ekman 1996). It should be noted here that the former centre of the Barents Sea ice sheet as modelled in this approach (Fig. 1) is located around 200 km SE of the Svalbard Archipelago. Comparing the predicted radial velocities for ice models ONSET1 and ONSET2, we observe a decrease in velocity by about 40–50 per cent for a delayed onset of the glaciation for all earth models considered.

Similar results apply along profile (b), indicating ongoing uplift over western Spitsbergen and minor subsidence in the western Barents Sea. Again, a delayed onset of glaciation results in a significant reduction in present-day radial velocities along the profile, with uplift rates lowered by about 0.5–1.5 mm a^{-1}, depending on the stiffness of the upper mantle.

Finally, radial velocities along profile (c) show uplift rates up to 10 mm a^{-1} close to the former centre of the Fennoscandian ice dome. Here the uplift rates are largest for earth model 120/94, resulting from the longer characteristic relaxation time of the stiffer upper mantle. No differences arise from the different ice models. Thus, the modified glaciation history

for the Barents Sea again influences the isostatic adjustment process only locally.

We conclude that we can resolve the delayed onset of glaciation in the Barents Sea proposed by ice model ONSET2 using present-day radial velocities. This result agrees with the inferences of Mitrovica & Davis (1995), who reported differences of up to 0.8 mm a^{-1} resulting from their ice model #3, using a delayed onset of *all* Pleistocene ice sheets relative to ice model #2, featuring a glaciation phase similar to the one in ice model ONSET1.

4.3 Present-day free air gravity anomaly

In this section the influence of a delayed onset of the growth of the Barents Sea ice sheet on predictions of the free air gravity anomaly (hereafter referred to as 'FAGA') is studied. Therefore, we predict FAGAs over the centre of the formerly glaciated areas of the Barents Sea and Scandinavia (Fig. 9) for a set of earth models with lithosphere and upper-mantle properties as described in Section 2.2 and η_{LM} ranging from 10^{21} to 10^{23} Pa s.

In the central Barents Sea we predict a peak FAGA ranging from 0 to -4.7 mGal with increasing η_{LM} for ice model ONSET1. These values are about 50 per cent smaller than values reported from the Gulf of Bothnia (Mitrovica & Davis 1995). Using ice model ONSET2, the predictions are reduced to 0 to -2 mGal with increasing η_{LM}. As observed in Mitrovica & Davis (1995) for the Gulf of Bothnia and James Bay (center of former Laurentian ice dome) the difference in the FAGA between the two adopted ice models increases with increasing η_{LM}.

In the Gulf of Bothnia the peak FAGA ranges from -1.5 to -16 mGal for earth models with η_{LM} ranging from 10^{21} to 10^{23} Pa s and ice model ONSET1. The predictions for ice model ONSET2 differ only slightly from these results. As a consequence we can predict the observed FAGA over the Gulf of Bothnia mentioned by Balling (1980) (shaded area in Fig. 9) only with earth models having a two orders of magnitude increase in mantle viscosity and a relatively stiff upper mantle. We note that the predicted FAGA is generally smaller than the values reported by Mitrovica & Davis (1995), which is a consequence of the recalibration of the ^{14}C timescale with its shift of the LGM.

We conclude that the assumption of a delayed glaciation phase in the Barents Sea significantly influences predictions of the FAGA in this area, but, as already shown using relative-sea-level predictions (Sections 4.2.1 and 4.2.2), this effect is only minor for locations further away, for example the Gulf of Bothnia. The total value of the predicted FAGA in the Barents Sea, not exceeding -5 mGal, raises the question whether this value can be measured accurately.

4.4 Palaeobathymetry

In the last section we derive a palaeobathymetry map of the Barents Sea and compare our result with the palaeobathymetry maps shown in Lambeck (1995). Therefore, a palaeotopography $TP(\theta, \phi, t)$ is derived on the basis of the present-day topography $T(\theta, \phi)$, and the sea level $S(\theta, \phi, t)$, using the relation

$$TP(\theta, \varphi, t) = T(\theta, \varphi) - S(\theta, \varphi, t) + S(\theta, \varphi, t=0). \quad (9)$$

Here $S(\theta, \phi, t)$ can be derived from (8) setting $C(\theta, \phi, t)$ equal to one everywhere. The related palaeobathymetry is the part of TP below sea level at the corresponding epoch.

We have calculated a palaeobathymetry corresponding to 28 ka BP based on earth model 120/74 and ice model ONSET2. It is redrawn, together with the present-day bathymetry of this area, in Fig. 10. Comparing both bathymetries, we find two important results. (1) The shallower parts of the northern Barents Sea, e.g. Spitsbergenbanken, Storbanken and the offshore areas around the Svalbard Archipelago and Franz Joseph Land, were very shallow or even exposed at 28 ka BP due to the eustatic sea-level fall on the one hand and to the forebulge uplift related to the Fennoscandian ice sheet on the other. These results essentially agree with the palaeobathymetries derived by Lambeck (1995). We note that, despite the use of different ice models and especially different time histories [in Lambeck (1995) the Barents Sea remained ice free during the entire last glaciation cycle], there is a

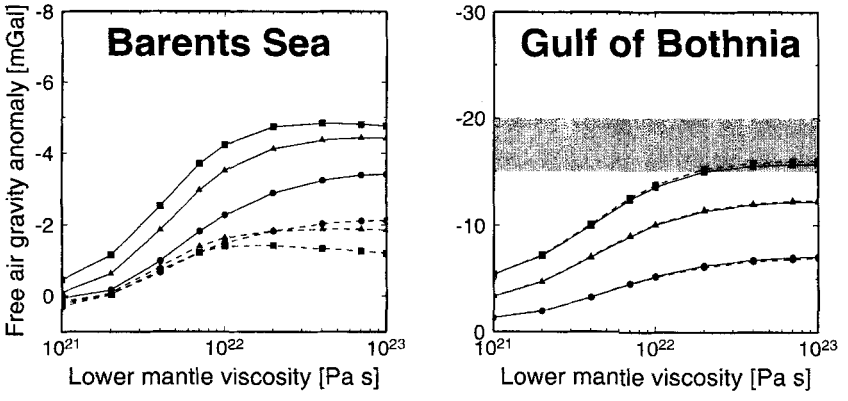

Figure 9. Calculated present-day free air gravity anomalies as a function of lower-mantle viscosity at former centres of the ice sheets over the Barents Sea (75°N, 38°W) and Fennoscandia (Gulf of Bothnia, 65°N, 24.5°W). Calculations apply to ice models ONSET1 (solid lines) and ONSET2 (dashed lines) and earth models with 120 km thick elastic lithosphere, upper-mantle viscosities of 4×10^{20} Pa s (circles), 7×10^{20} Pa s (triangles) and 10^{21} Pa s (squares), and lower-mantle viscosities as shown on the abcissa. The shaded area indicates ranges of observed present-day peak free air gravity anomalies (see text for details).

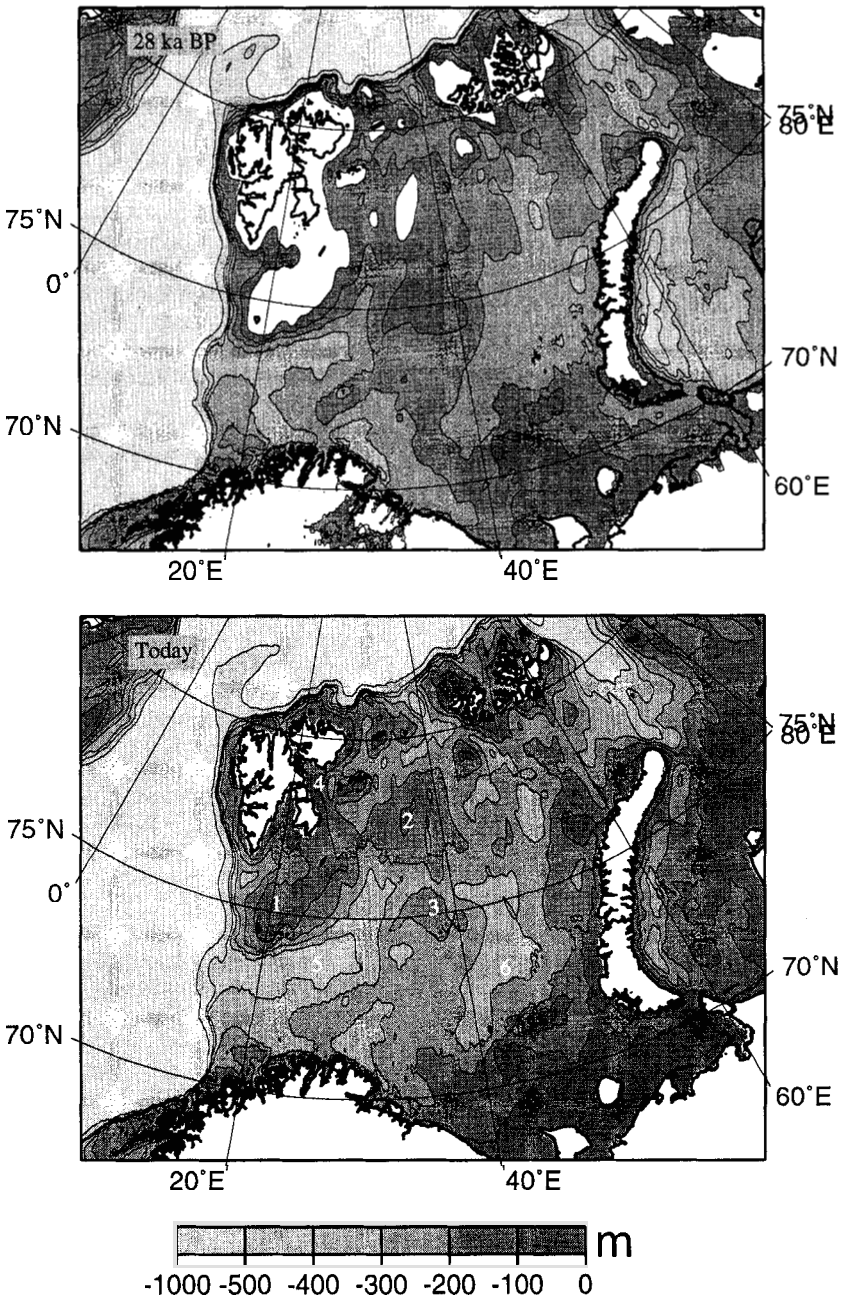

Figure 10. Present-day bathymetry (lower panel) and palaeobathymetry at 28 ka BP (upper panel) for the Barents Sea. Calculations for palaeobathymetry apply to ice model ONSET2 and earth model 120/74. Areas shown in white are above mean sea level at the corresponding epoch. The geographical locations indicated by numbers are Spitsbergenbanken (1), Storbanken (2), Sentralbanken (3), Hinlopenstretet (4), Bjørnøyrenna (5) and central deep (6).

remarkable agreement concerning the areas around the Svalbard Archipelago and Franz Joseph Land, which were raised above sea level at corresponding epochs. (2) The water depth in the southernmost Barents Sea around the central deep was deeper at around 28 ka BP than at present due to the deformation in the close vicinity of the Fennoscandian ice sheet.

5 CONCLUDING REMARKS

We can summarize our results in terms of the objectives raised in the introduction.

(1) A delayed onset of the glaciation in the Barents Sea with an accumulation phase starting shortly before the LGM can *significantly* influence the isostatic adjustment in the Barents Sea. The influence is a *regional* effect, thus the glacial isostatic adjustment in the area of the former Fennoscandian ice sheet is insensitive to the delayed growth of the Barents Sea ice sheet.

(2) From the observables considered, we find that relative sea levels are the most sensitive for detecting differences in the glaciation phase. Here especially, observations prior to the LGM can provide a useful constraint on the onset of glaciation. Additionally, observations of both present-day vertical velocities and gravity anomalies resolve the glaciation

history. However, the latter observable in particular is much smaller than in other previously glaciated areas and therefore difficult to observe.

(3) Finally we support the hypothesis of Hald *et al.* (1990) and Mangerud *et al.* (1992) that the Barents Sea was an essentially marine environment shortly before the LGM and thus provided additional emerged areas above sea level to initiate the growth of a large marine-based ice sheet.

ACKNOWLEDGMENTS

The numerical transformation routines used to expand variables into their spherical harmonic coefficients were provided by Dr Helmut Harder, University of Göttingen, Germany. I gratefully acknowledge this help. Constructive comments from Dr Paul Johnston on an earlier version of this manuscript are also gratefully acknowledged. The points raised by an anonymous reviewer helped to improve this paper. This work is partially funded by the ARC grant No. IRFG9608. The figures in this paper were drawn using the GMT graphics package [for details see Wessel & Smith (1991)].

REFERENCES

Balling, N., 1980. The land uplift in Fennoscandia, gravity field anomalies and isostasy, in *Earth Rheology, Isostasy, and Eustasy,* pp. 297–321, ed. Mörner, N.A., John Wiley & Sons, Chichester.

Bard, E., Hamelin, B., Fairbanks, R.G. & Zindler, A., 1990. Calibration of the ^{14}C timescale over the past 30.000 years using mass spectrometric U–Th ages from Barbados corals, *Nature,* **345,** 405–410.

Biot, M.A., 1962. Mechanics of deformation and acoustic propagation in porous media, *J. appl. Phys.,* **33,** 1482–1498.

Chappell, J. & Shackleton, N.J., 1986. Oxygen isotopes and sealevel, *Nature,* **324,** 137–140.

Denton, G.H. & Hughes, T.J., 1981. *The Last Great Ice Sheets,* John Wiley & Sons, New York, NY.

Donner, J., 1980. The determination and dating of synchronous late Quaternary shorelines in Fennoscandia, in *Earth Rheology, Isostasy, and Eustasy,* pp. 285–293, ed. Mörner, N.-A., J. Wiley, Chichester.

Dziewonski, A.M. & Anderson, D.L., 1981. Preliminary reference Earth model, *Phys. Earth planet. Inter.,* **25,** 279–356.

Ekman, M., 1996. A consistent map of the postglacial uplift of Fennoscandia, *Terra Nova,* **8,** 158–165.

Elverhøi, A., Fjeldskaar, W., Solheim, A., Nyland-Berg, M. & Russworm, L., 1993. The Barents Sea ice sheet—a model of its growth and decay during the last glacial maximum, *Quat. Sci. Rev.,* **12,** 863–873.

Fairbanks, R.G., 1989. A 17000-year glacio–eustatic sea-level record: influence of glacial melting rates on the younger Dryas event and deep–ocean circulation, *Nature,* **342,** 637–642.

Farell, W.A., 1972. Deformation of the Earth by surface loads, *Rev. Geophys. Space Sci.,* **10,** 761–797.

Farrell, W.E. & Clark, J.A., 1976. On postglacial sea level, *Geophys. J. R. astr. Soc.,* **46,** 647–667.

Hald, M., Danielsen, T.K. & Lorentzen, S., 1990. Middle and late Weichselian stratigraphy in shallow drilling from the southwestern Barents Sea: foraminiferal, amino acid and radiocarbon evidence, *Geophys. Res. Lett.,* **70,** 241–257.

Han, D. & Wahr, J., 1995. The viscoelastic relaxation of a realistically stratified Earth, and a further analysis of postglacial rebound, *Geophys. J. Int.,* **120,** 287–311.

Heiskanen, W.A. & Moritz, H., 1967. *Physical Geodesy,* Freeman, San Francisco, CA.

Johnston, P., 1993. The effect of spatially non–uniform water loads on prediction of sea-level change, *Geophys. J. Int.,* **114,** 615–634.

Kaufmann, G., 1995. Zur Auflösbarkeit lateraler Heterogenitäten im Erdmantel durch nacheiszeitliche Landhebungen am Beispiel der nördlichen Barentssee, *PhD thesis,* Institut für Planetologie, Westfälische Wilhelms-Universität, Münster.

Kaufmann, G. & Wolf, D., 1996. Deglacial land emergence and lateral upper-mantle heterogeneity in the Svalbard Archipelago—II. Extended results for high-resolution load models, *Geophys. J. Int.,* **127,** 125–140.

Lambeck, K., 1995. Constraints on the late Weichselian ice sheet over the Barents Sea from observations of raised shorelines, *Quat. Sci. Rev.,* **14,** 1–16.

Longman, I.M., 1962. A Green's function for determining the deformation of the Earth under surface mass loads, *J. geophys. Res.,* **67,** 845–850.

Love, A.E.H., 1911. *Some Problems of Geodynamics,* Cambridge University Press, Cambridge.

Mangerud, J., Bondevik, S., Ronnert, L. & Salvigsen, O., 1992. Shore displacement and marine limits on Edgeøya and Barentsøya, eastern Svalbard, *Lundqua Report,* **35,** 51–60.

Mitrovica, J.X. & Davis, J.L., 1995. The influence of a finite glaciation phase on predictions of post-glacial isostatic adjustment, *Earth planet. Sci. Lett.,* **136,** 343–361.

Mitrovica, J.X. & Peltier, W.R., 1989. Pleistocene deglaciation and the global gravity field, *J. geophys. Res.,* **94,** 13 651–13 671.

Mitrovica, J.X. & Peltier, W.R., 1991. On postglacial geoid subsidence over the equatorial oceans, *J. geophys. Res.,* **96** (B12), 20 053–20 071.

Mitrovica, J.X., Davis, J.L. & Shapiro, I.I., 1994. A spectral formalism for computing 3-D deformations due to surface loads 2. Present-day glacial isostatic adjustment, *J. geophys. Res.,* **99** (B4), 7075–7101.

Munk, W.H. & MacDonald, G.J.F., 1960. *The Rotation of the Earth: A Geophysical Discussion,* Cambridge University Press, London.

Nakada, M. & Lambeck, K., 1987. Glacial rebound and relative sea-level variations: a new appraisal, *Geophys. J. R. astr. Soc.,* **90,** 171–224.

Peltier, W.R., 1974. The impulse response of a Maxwell Earth, *Rev. Geophys. Space Sci.,* **12** (4), 649–669.

Peltier, W.R. & Andrews, J.T., 1976. Glacial-isostatic adjustment – I. The forward problem, *Geophys. J. R. astr. Soc.,* **46,** 605–646.

Peltier, W.R. & Tushingham, A.M., 1989. Global sea level rise and the greenhouse effect: might they be connected?, *Science,* **244,** 806–810.

Tushingham, A.M. & Peltier, W.R., 1991. Ice-3G: a new global model of late Pleistocene deglaciation based upon geophysical predictions of post-glacial relative sea level change, *J. geophys. Res.,* **96,** 4497–4523.

Tushingham, A.M. & Peltier, W.R., 1992. Validation of the Ice-3G model of Würm–Wisconsin deglaciation using a global data base of relative sea level histories, *J. geophys. Res.,* **97,** 3285–3304.

Wessel, P. & Smith, W.H.F., 1991. Free software helps map and display data, *EOS, Trans. Am. geophys. Un.,* **72,** 441–446.

Wu, P. & Peltier, W.R., 1983. Glacial isostatic adjustment and the free air gravity anomaly as a constraint on deep mantle viscosity, *Geophys. J. R. astr. Soc.,* **74,** 377–449.